R-matrix calculation of electron collisions with electronically excited O$_2$ molecules

Motomichi Tashiro* and Keiji Morokuma

Department of Chemistry, Emory University, 1515 Dickey Drive, Atlanta, Georgia 30322, USA

Jonathan Tennyson

Department of Physics and Astronomy, University College London, London WC1E 6BT, United Kingdom

Low-energy electron collisions with O$_2$ molecules are studied using the fixed-bond *R*-matrix method. In addition to the O$_2$ $X\,^3\Sigma_g^-$ ground state, integrated cross sections are calculated for electron collisions with the $a\,^1\Delta_g$ and $b\,^1\Sigma_g^+$ excited states of O$_2$ molecules. Thirteen target electronic states of O$_2$ are included in the model within a valence configuration interaction representations of the target states. Elastic cross sections for the $a\,^1\Delta_g$ and $b\,^1\Sigma_g^+$ excited states are similar to the cross sections for the $X\,^3\Sigma_g^-$ ground state. As in case of excitation from the $X\,^3\Sigma_g^-$ state, the O$_2^-$ Π_u resonance makes the dominant contribution to excitation cross sections from the $a\,^1\Delta_g$ and $b\,^1\Sigma_g^+$ states. The magnitude of excitation cross sections from the $a\,^1\Delta_g$ state to the $b\,^1\Sigma_g^+$ state is about ten times larger than the corresponding cross sections from the $X\,^3\Sigma_g^-$ to the $b\,^1\Sigma_g^+$ state. For this $a\,^1\Delta_g \rightarrow b\,^1\Sigma_g^+$ transition, our cross section at 4.5 eV agrees well with the available experimental value. These results should be important for models of plasma discharge chemistry which often requires cross sections between the excited electronic states of O$_2$.

I. INTRODUCTION

An understanding of electron collision processes with oxygen molecules is important because of its role in the chemistry of electrical discharge and the upper atmosphere. In recent attempts to operate an electrical discharge oxygen-iodine laser, a population inversion of iodine atoms was achieved by a near resonant energy transfer via the O$_2(a\,^1\Delta_g)$+I($^2P_{3/2}$)$\leftrightarrow$O$_2(X\,^3\Sigma_g^-)$+I($^2P_{1/2}$) process. In contrast to the traditional liquid chemistry singlet oxygen generator [1], recent studies [2,3] utilize flowing electric discharges where electron collisions with O$_2$ excited electronic states can be important [4,5]. In such conditions, even highly excited metastable states of O$_2(c\,^1\Sigma_u^-,\ A'\,^3\Delta_u,\ A\,^3\Sigma_u^+)$ may play roles [6], in addition to the lower O$_2$ $a\,^1\Delta_g$ and $b\,^1\Sigma_g^+$ excited states.

However, most previous work has concentrated on electron collisions with the O$_2(X\,^3\Sigma_g^-)$ ground state, so our knowledge of electron impact transitions from the O$_2 a\,^1\Delta_g$ and $b\,^1\Sigma_g^+$ excited states is limited. The past experimental and theoretical works concerning electron O$_2(X\,^3\Sigma_g^-,\ a\,^1\Delta_g)$ collisions were summarized by Brunger and Buckman [7]. One work on the excited electronic states is measurement of differential and integral cross sections at 4.5 eV for excitation from the O$_2$ $a\,^1\Delta_g$ state to the $b\,^1\Sigma_g^+$ state by Hall and Trajmar [8]. Their value is more than an order of magnitude larger than that for the $X\,^3\Sigma_g^-\rightarrow b\,^1\Sigma_g^+$ cross section. Also, Khakoo *et al.* [9] studied the energy-loss spectrum for electron impact excitation on discharged O$_2$ and assigned the transitions O$_2 a\,^1\Delta_g$ $(v=0)\rightarrow$O$_2$ $^1\Pi_u$ $(v'=0,1,\dots 7)$. Burrow [10] and Belić and Hall [11] studied dissociative electron attachment with the O$_2$ $a\,^1\Delta_g$ state. The later authors found

that dissociation proceeds to three different limits, O$^-$(^2P)+O(^3P), O$^-$(^2P)+O(^1D) and O$^-$(^2P)+O(^1S).

In contrast to the situation in electron collisions with the excited oxygen molecule, a lot of work has been performed on the ground state O$_2$, both experimental [12–16] and theoretical [12,14–21]. Notably, Noble, Burke, and their co-workers extensively applied their *R*-matrix method to the electron O$_2$ collision problems during 1992–1996 [14–16,18–21]. They studied electronic excitation processes from the O$_2(X\,^3\Sigma_g^-)$ ground state to the $a\,^1\Delta_g$, $b\,^1\Sigma_g^+$, $c\,^1\Sigma_u^-$, $A'\,^3\Delta_u$ and $A\,^3\Sigma_u^+$ states using the fix-bond *R*-matrix method [18,19] and applied the nonadiabatic *R*-matrix method to vibrational excitations process of the $X\,^3\Sigma_g^-(v=0)\rightarrow X\,^3\Sigma_g^-(v=0-4)$ transitions [20,21]. They also calculated differential cross sections for elastic electron collisions of the $X\,^3\Sigma_g^-$ state [15] as well as impact excitations from the $X\,^3\Sigma_g^-$ state to the $a\,^1\Delta_g$ and $b\,^1\Sigma_g^+$ states [14]. The effect of nuclear motion was included in the former elastic cross sections by vibrational averaging of the *T* matrix [15]. Other than these *R*-matrix calculations, Teillet-Billy *et al.* [12] applied effective range theory (ERT) to excitations from the $X\,^3\Sigma_g^-$ to the $a\,^1\Delta_g$ and $b\,^1\Sigma_g^+$ states. Because of the different treatment of the O$_2^-$ resonances, the ERT results deviate from the *R*-matrix cross sections at energies above 5 eV.

Given the importance of electron collisions with excited O$_2$ molecules, we perform *R*-matrix calculations for electron O$_2(a\,^1\Delta_g, b\,^1\Sigma_g^+)$ collisions. We chose the *R*-matrix method because it has been successfully applied to many electron-molecule collisions including e-N$_2$, N$_2$O and H$_2$O [22–24]. The fixed-bond method was employed in this work, because it gave reasonably good results in previous studies [17–19] for transitions from the O$_2$ $X\,^3\Sigma_g^-$ state to the $a\,^1\Delta_g$, $b\,^1\Sigma_g^+$ state, and the "6 eV states" $(c\,^1\Sigma_u^-+A'\,^3\Delta_u+A\,^3\Sigma_u^+)$. In addition to these six low lying O$_2$ target states, previous calculations included three higher excited target states of O$_2$ $B\,^3\Sigma_u^-$, $1\,^1\Delta_u$, and $f'\,^1\Sigma_u^+$, in order to improve quality of the *R*-matrix

*Email address: tashiro@euch4e.chem.emory.edu

calculations [18,19]. In this work, we use a valence complete active space description of the O_2 target states and add other valence target states, $1\,^1\Pi_g, 1\,^3\Pi_g, 1\,^1\Pi_u, 1\,^3\Pi_u$, in our calculations. Since excitation energies of some of these states are lower than those of $B\,^3\Sigma_u^-$, $1\,^1\Delta_u$, and $f'\,^1\Sigma_u^+$ states, some improvement can be expected by inclusion of these extra Π target states. In principle, a complete valence active space is not sufficient for the description of these targets, because some of them are mixed with $n=3$ Rydberg states as described in Buenker and Peyerimhoff [25,26]. Since expansion of this active space increases the calculation cost considerably, we limit ourselves here the inclusion of the valence states to test the effects of the higher excited states.

In this paper, details of the calculations are presented in section II, and we discuss the results in Sec. III comparing our results with previous theoretical and available experiments. Then the summary is given in Sec. IV.

II. THEORETICAL METHODS

The R-matrix method has been described extensively in the previous literature [23,24,27], so here we only repeat the outline of the method. In this method, configuration space is divided by two regions according to the distance r_{N+1} of the scattering electron and the center of mass of the target molecule having N electrons. In the inner region $r_{N+1} < a$, the $N+1$ electrons problem is solved by usual quantum chemistry method with slight modifications to account for existence of boundary at $r_{N+1} = a$. In the inner region, the total $N+1$ electrons wave functions are represented by N-electron configuration interaction (CI) target wave functions augmented by diffuse functions. Here the target wave functions are contained in the sphere $r_{N+1} < a$, whereas the diffuse functions overlap the boundary at $r_{N+1} = a$ in order to describe the scattering electron. In the outer region $r_{N+1} > a$, the problem is reduced to single electron scattering, ignoring exchange of the scattering electron with the target electrons. Interaction of the scattering electron and the target is considered through static multipolar interaction terms which introduce interchannel couplings. The wave functions obtained in the inner region are converted to the R matrix at the boundary $r_{N+1} = a$, then the coupled radial Schrödinger equations are solved so as to extract scattering information at the asymptotic region.

In the inner region, the $N+1$ electronic wave functions are expanded as,

$$\Psi = \mathcal{A} \sum_{ij} \Phi_i(1,\ldots,N;R) u_j(N+1;R) a_{ij}$$
$$+ \sum_q X_q(1,\ldots,N+1;R) b_q, \qquad (1)$$

where $\mathcal{A}$ is an antisymmetrization operator, Φ_i are the N electron target CI wave functions, u_j are the diffuse functions representing wave functions of a scattering electron, and X_q are bound $N+1$ electron wave functions, while a_{ij} and b_q are variational coefficients. In this expression, the first term represents the scattering of an electron from and to the asymptotic region. The second summation involves purely L^2 integrable terms. In addition to the target molecular orbitals
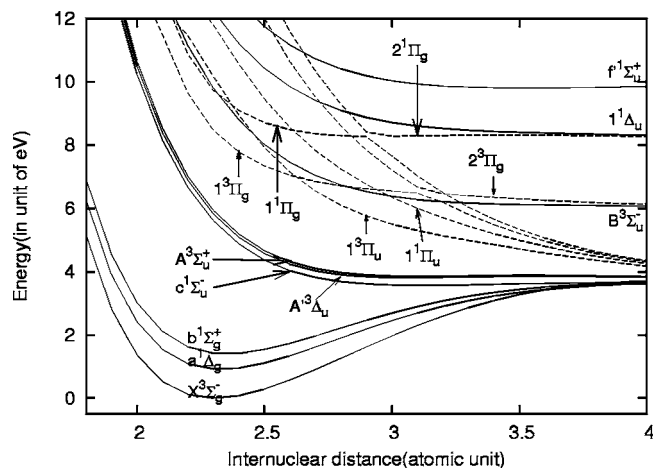

FIG. 1. Potential energy curves of the O_2 electronic states. The equilibrium distance of the $X\,^3\Sigma_g^-$ state, $R=2.3a_0$ is used in our R-matrix calculations.

included in the CI wave functions in the first summation, some extra target virtual orbitals are usually included in X_q in order to account for short range polarization effects.

We used a modified version of the polyatomic programs in the UK molecular R-matrix codes [27]. These programs utilize Gaussian type orbitals (GTO) to represent target molecule as well as a scattering electron. Although most of past R-matrix works on electron O_2 collisions had employed the diatomic modules using Slater type orbitals (STO) obtained by Hartree Fock (HF) calculation, we select GTO mainly because of simplicity of the input and availability of basis functions. The state averaged complete active space SCF (SA-CASSCF) orbitals are imported from the target calculations with MOLPRO suites of programs [28]. This employment of SA-CASSCF orbitals improves the vertical excitation energies of the O_2 target states compared to the energies obtained using HF orbitals. These target orbitals are constructed from the $[5s, 3p]$ contracted basis of Dunning [29] augmented by a d function with exponent 1.8846, as in Sarpal *et al.* [30]. In the R-matrix calculations, we included 13 target states; $X\,^3\Sigma_g^-$, $a\,^1\Delta_g$, $b\,^1\Sigma_g^+$, $c\,^1\Sigma_u^-$, $A'\,^3\Delta_u$, $A\,^3\Sigma_u^+$, $B\,^3\Sigma_u^-$, $1\,^1\Delta_u$, $f'\,^1\Sigma_u^+$, $1\,^1\Pi_g$, $1\,^3\Pi_g$, $1\,^1\Pi_u$, and $1\,^3\Pi_u$, where the last 4 Π states were not included in previous calculations. The potential energy curves of these target electronic states are shown in Fig. 1 for reference. Further details of these target electronic states can be found in Saxon and Liu [31] and Minaev and Minaeva [32] for example. In our fixed-bond R-matrix calculations, these target states are evaluated at the equilibrium bond length $R=2.3a_0$ of the $O_2\ X\,^3\Sigma_g^-$ ground electronic state. Note that all calculations were performed with D_{2h} symmetry because of restriction of the polyatomic UK R-matrix codes, though natural symmetry of this system is $D_{\infty h}$.

The radius of the R-matrix sphere a was chosen to be 10 a_0 in our calculations. In order to represent the scattering electron, we included diffuse gaussian functions up to $l=5$ with nine functions for $l=0$, seven functions for $l=1-3$ and 6 functions for $l=4$ and 5. The exponents of these Gaussians were fitted using the GTOBAS program [33] in the UK

TABLE I. Division of the orbital set in each symmetry.

Symmetry	A_g	B_{2u}	B_{3u}	B_{1g}	B_{1u}	B_{3g}	B_{2g}	A_u
Valence	$1-3a_g$	$1b_{2u}$	$1b_{3u}$		$1-3b_{1u}$	$1b_{3g}$	$1b_{2g}$	
Extra virtual	$4a_g$	$2b_{2u}$	$2b_{3u}$	$1b_{1g}$	$4b_{1u}$	$2b_{3g}$	$2b_{2g}$	$1a_u$
Continuum	$5-38a_g$	$3-35b_{2u}$	$3-35b_{3u}$	$2-17b_{1g}$	$5-37b_{1u}$	$3-18b_{3g}$	$3-18b_{2g}$	$2-17a_u$

R-matrix codes. Details of the fitting procedure are the same as in Faure *et al.* [33]. We constructed the $N+1$ electron configurations from the orbitals listed in Table I. The CI target wave functions are composed from the valence orbitals in Table I with the $1a_g$ and $1b_{1u}$ orbitals kept doubly occupied. The first terms in Eq. (1) are constructed from configurations of the form

$$1a_g^2 1b_{1u}^2\{2a_g 3a_g 1b_{2u} 1b_{3u} 2b_{1u} 3b_{1u} 1b_{3g} 1b_{2g}\}^{12}(^3B_{1g})$$
$$\times\{2b_{1g}\ldots 17b_{1g}\}^1(^2A_g), \qquad (2)$$

here we assume that the total symmetry of this 17 electrons system is ^2A_g. The first four electrons are always kept in the $1a_g$ and $1b_{1u}$ orbitals, then the next 12 electrons are distributed over the valence orbitals with restriction of target state symmetry, $^3B_{1g}$ symmetry of the O_2 ground state in this case. The last electron, the scattering electron, occupies one of the diffuse orbitals, B_{1g} symmetry in this example. To complete the wave function with the total symmetry ^2A_g, we also have to include configurations with the other target states combined with diffuse orbitals having appropriate symmetry in the same way as in the example. The second terms in Eq. (1) are constructed from configurations

$$1a_g^2 1b_{1u}^2\{2a_g 3a_g 1b_{2u} 1b_{3u} 2b_{1u} 3b_{1u} 1b_{3g} 1b_{2g}\}^{12}(^3B_{1g})$$
$$\times\{1b_{1g}\}^1(^2A_g), \qquad (3)$$

where the scattering electron occupies a bound $1b_{1g}$ extra virtual orbital, instead of the diffuse continuum orbitals in the expression (2). As in Table I, we included one extra virtual orbital for each symmetry. The second terms in Eq. (1) also contain configurations of the form

$$1a_g^2 1b_{1u}^2\{2a_g 3a_g 1b_{2u} 1b_{3u} 2b_{1u} 3b_{1u} 1b_{3g} 1b_{2g}\}^{13}(^2A_g). \quad (4)$$

In this case, the last 13 electrons including the scattering electron are distributed over the valence orbitals with the restriction of ^2A_g symmetry. In this way, the number of configurations generated for a specific total symmetry is typically about 17 000, though the final dimension of the inner region Hamiltonian is reduced to be about 500 by using CI target contraction and prototype CI expansion method [34].

In order to obtain the integral cross sections for the electron O_2 collisions, the R-matrix calculations were performed over all eight irreducible representations of D_{2h} symmetry, A_g, B_{2u}, B_{3u}, B_{1g}, B_{1u}, B_{3g}, B_{2g}, and A_u with both doublet and quartet spin multiplicity.

III. RESULTS AND DISCUSSION

Figure 1 shows the potential energy curves of the O_2 target states. These curves were calculated by the SA-CASSCF method which was used in the actual R-matrix calculations. Although not included in our R-matrix calculations, we also include the curves for the $O_2(2 \,^{1,3}\Pi_g)$ states for reference. Table II compares vertical excitation energies from the present calculations with previous HF STO results. Compared to the experimentally estimated values, our results are of the same quality for the O_2 $a\,^1\Delta_g$ state and are slightly worse, 0.05 eV, than the HF STO result for the $b\,^1\Sigma_g^+$ state. However, the excitation energies are improved by about 0.1 eV for the 6 eV states; $c\,^1\Sigma_u^-$, $A'\,^3\Delta_u$, and $A\,^3\Sigma_u^+$. For the higher three electronic states, the improvement is about 1 eV. Though discrepancies with the experimental values are still not small, 0.22 eV for the $b\,^1\Sigma_g^+$ state and 0.45 eV for the $A'\,^3\Delta_u$ state for examples, we believe that our choice of

TABLE II. Comparison of the vertical excitation energies at $R=2.3a_0$ from the present CASSCF GTO calculations with previous work of Middleton *et al.* (see Ref. [14]) as well as experimental values quoted in Teillet-Billy *et al.* (see Ref. [12]). The unit of energy is electron-volts.

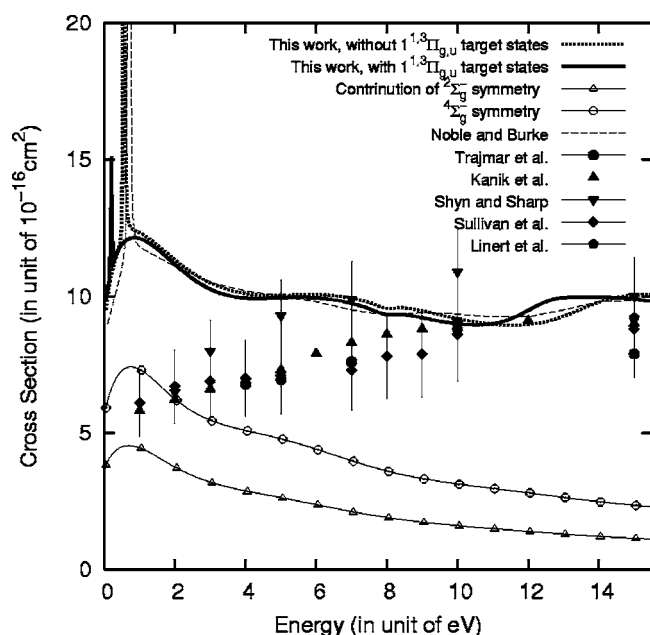| State	Present CASSCF GTO	Previous HF STO	Experimental values
$X\,^3\Sigma_g^-$	0.00	0.00	0.00
$a\,^1\Delta_g$	0.93	0.93	0.98
$b\,^1\Sigma_g^+$	1.43	1.47	1.65
$c\,^1\Sigma_u^-$	5.60	5.49	6.12
$A'\,^3\Delta_u$	5.82	5.68	6.27
$A\,^3\Sigma_u^+$	5.93	5.81	6.47
$B\,^3\Sigma_u^-$	9.80	10.86	9.25
$1\,^1\Delta_u$	12.23	13.16	11.8
$f'\,^1\Sigma_u^+$	13.57	14.67	13.25

FIG. 2. The elastic cross sections of the O_2 $X\,^3\Sigma_g^-$ state. The thick full line represents cross sections obtained by 13 target states calculation including $1\,^{1,3}\Pi_{g,u}$ target states. The thick dotted line is the cross sections including nine target states without $1\,^{1,3}\Pi_{g,u}$ target states. The partial cross sections from the 13 target states calculation are represented by thin full lines marked with open symbols. Symmetries with minor contributions are not shown in the figure. For comparisons, we also include the previous R-matrix results of Noble and Burke (see Ref. [18]), the experimental cross sections of Trajmar *et al.* (see Ref. [39]), Kanik *et al.* (see Ref. [40]), Shyn and Sharp (see Ref. [41]), Sullivan *et al.* (see Ref. [42]), and Linert *et al.* (see Ref. [43]).

the GTO basis set and the CAS space is satisfactory for the present R-matrix calculations considering the differences with the previous HF STO results.

In Figs. 2–5, the cross sections for the transitions from the $O_2(X\,^3\Sigma_g^-)$ ground state are shown. These cross sections were previously calculated using the R-matrix method, but with a different basis set and target descriptions [17,18]. In Fig. 2, we compare our elastic scattering cross sections for the $X\,^3\Sigma_g^-$ state with the previous theoretical and experimental results. The theoretical elastic scattering cross sections are quite similar in shape and magnitude each other. There is a sharp peak around 0.5 eV in each theoretical cross section, which comes from the $O_2^-\,^2\Pi_g$ resonance. In our calculation with 13 target states including four extra Π targets, this $^2\Pi_g$ resonance is located at 0.196 eV and the width is 0.001 34 eV. When the number of targets are reduced to 9 by removing the Π target states, the location of the resonance is shifted to 0.548 eV with a width of 0.01 61 eV. The later resonance parameters with nine target states are closer to the results of the previous calculations, reflecting inclusion of the same number of the target states. When our results are compared to the experimentally measured elastic cross sections, agreement is good for energy above 10 eV but is poorer at lower scattering energy below 5 eV. At 1 eV, the theoretical cross section is about a factor of 2 larger than the experimental results. This situation mirrors that in the previ-
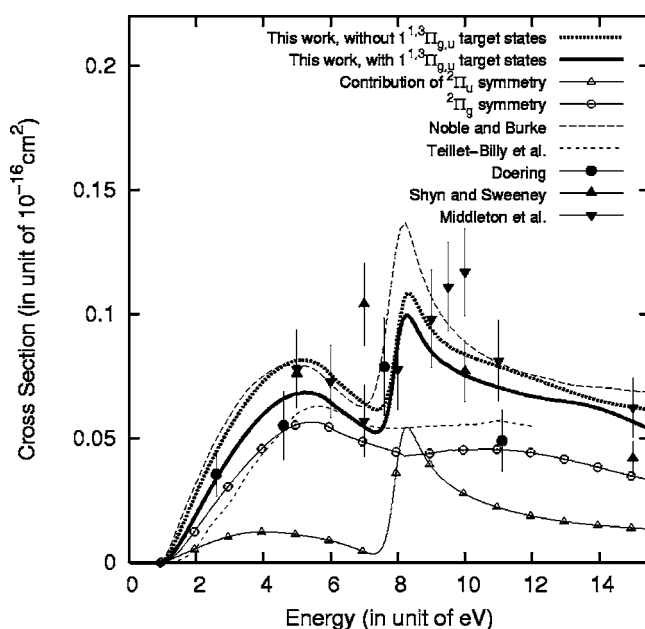

FIG. 3. The excitation cross section from the O_2 $X\,^3\Sigma_g^-$ state to the $a\,^1\Delta_g$ state. Our results are shown in thick full and dotted lines as in Fig. 2. The partial cross sections of $^2\Pi_{g,u}$ symmetries are also shown as thin full lines marked with open symbols. For comparison, we include the previous R-matrix results of Noble and Burke (see Ref. [18]), the ERT calculations of Teillet-Billy *et al.* (see Ref. [12]), the experimental cross sections of Doering (see Ref. [44]), Shyn and Sweeney (see Ref. [45]), and Middleton *et al.* (see Ref. [13]).

ous R-matrix calculations. As discussed in Noble and Burke [18], this discrepancy is attributed to lack of long-range polarization effects in our and their model. To improve this low energy behavior of the elastic cross sections, we may need pseudostates method of Gillan *et al.* [35] and Gorfinkiel and Tennyson [36] for example.

Figures 3 and 4 show excitation cross sections from the $O_2 X\,^3\Sigma_g^-$ state to the $a\,^1\Delta_g$ and $b\,^1\Sigma_g^+$ states. In both figures, there is a pronounced peak in the cross sections around 8 eV which comes from the $O_2^-\,^2\Pi_u$ resonance located at 7.988 eV with its width being 0.906 eV. Compared to the previous R-matrix calculations of Noble and Burke [18], our cross sections with 13 target states are slightly smaller at all scattering energies. The peak height of our results around 8 eV is 30% smaller in excitation to the $a\,^1\Delta_g$ case and is 35% smaller in the $b\,^1\Sigma_g^+$ case. However, general feature of the cross section profiles are quite similar in our results and the previous R-matrix calculations. We also compare our results with the ERT results of Teillet-Billy *et al.* [12]. Their method relied on the existence of the $O_2^-\,^2\Pi_g$ resonance around 0.2 eV, but did not include the effect of the $O_2^-\,^2\Pi_u$ resonance located at 8 eV. Thus, their results and our cross sections agree well at low energy, below 6 eV, where the $^2\Pi_g$ symmetry mainly contributes to the total cross sections. However, the agreement is worse at energy range above 7 eV because of the $^2\Pi_u$ resonance contributions. In both $O_2(a\,^1\Delta_g)$ and $O_2(b\,^1\Sigma_g^+)$ cases, agreement with the experimental cross sections is modestly good in the energy regions
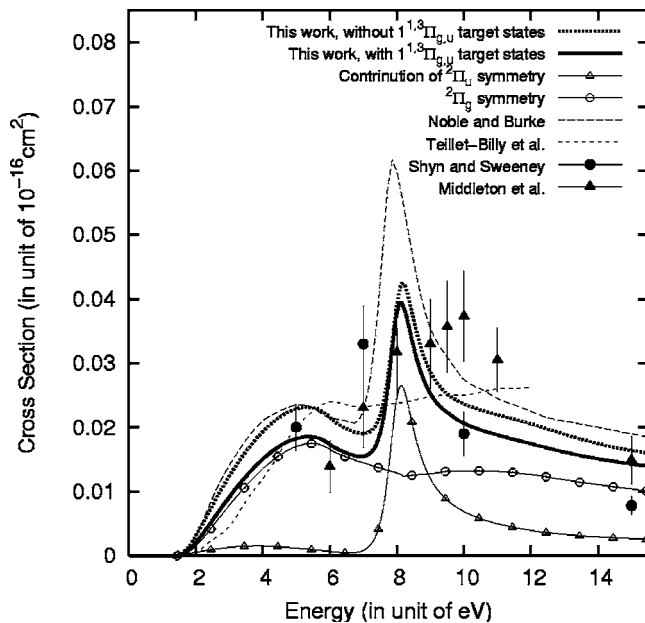
FIG. 4. The excitation cross section from the O_2 $X^3\Sigma_g^-$ state to the $b^1\Sigma_g^+$ state. Our results are shown in thick full and dotted lines as in Fig. 2. We include the previous theoretical results of Noble and Burke (see Ref. [18]), Teillet-Billy et al. (see Ref. [12]) and the experimental cross sections of Shyn and Sweeney (see Ref. [45]) and Middleton et al. (see Ref. [13]).

FIG. 5. The excitation cross sections from the O_2 $X^3\Sigma_g^-$ state to the 6 eV states which consist of the O_2 $c^1\Sigma_u^-$, $A'^3\Delta_u$, and $A^3\Sigma_u^+$ states. The total cross sections shown here are the sum of the individual cross sections of these three states. Our results for the total cross sections are shown in thick full and dotted lines as in Fig. 2. The individual excitation cross sections from 13 states calculations are shown as thin full lines marked with open symbols. We include the total cross sections from the previous R-matrix results of Noble and Burke (see Ref. [18]), the ERT calculations of Gauyacq et al. (see Ref. [37]), the experimental results of Teillet-Billy et al. (see Ref. [46]) and Green et al. (see Ref. [38]).

away from the resonance peak. As shown in the Figs. 3 and 4, the cross sections of Middleton et al. [13] have peak in energy region around 10 eV, which is 2 eV larger than the theoretical position. To resolve this discrepancy, we need to include the effect of nuclear motion in calculation as discussed in Higgins et al. [19].

Figure 5 shows excitation cross sections from the O_2 $X^3\Sigma_g^-$ state to the 6 eV states. These 6 eV states consist of the O_2 $c^1\Sigma_u^-$, $A'^3\Delta_u$, and $A^3\Sigma_u^+$ states. In order to compare with previous experimental measurements, we sum the cross sections for the transitions to these states. As in the case of transitions to the $a^1\Delta_g$ and $b^1\Sigma_g^+$ states in Figs. 3 and 4, a prominent peak exists around 8 eV in our results. The cause of this peak is the O_2^- $^2\Pi_u$ resonance located at 7.988 eV. Our results are quite similar in shape and magnitude to the previous R-matrix calculation of Noble and Burke [18], though the cross section peak at 8 eV is slightly lower in our case. The ERT results of Gauyacq et al. [37] are also shown in the figure. As discussed above, their cross sections do not have a peak around 8 eV because they did not include the O_2^- $^2\Pi_u$ resonance effects. Recently, Green et al. [38] measured the integral cross sections from the $X^3\Sigma_g^-$ state to the 6 eV states and discussed the discrepancy between the past theoretical results and their measurements. Though the theoretical cross sections have a peak around 8 eV, the experimental results do not show this peak nor the enhancement of the cross sections near 8 eV. Figure 5 compares our results with the experimental cross sections, which shows that the discrepancy still exists below 10 eV. This deviation may come from our use of fixed-bond approximation, because the equilibrium bond distances of 6 eV state are longer than those of
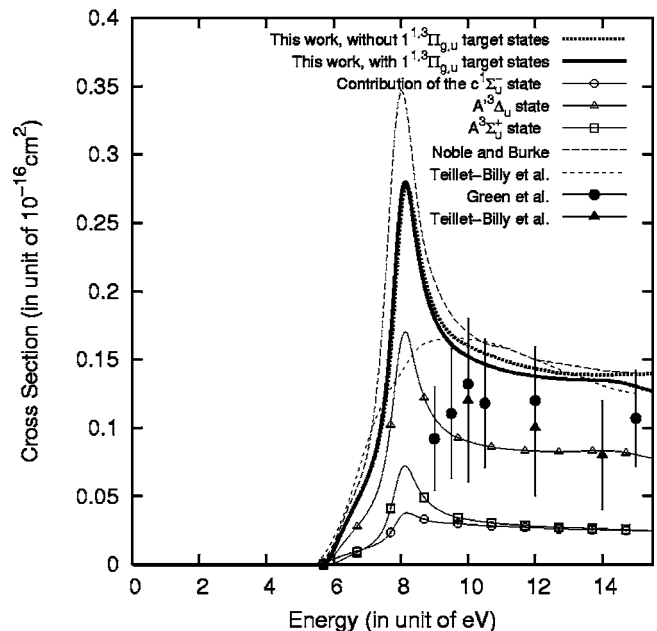
$X^3\Sigma_g^-$, $a^1\Delta_g$, and $b^1\Sigma_g^+$ states. In principle, we need to employ the nonadiabatic R-matrix method or vibrational averaging procedure to take into account those difference of the equilibrium distances. In this study, we limit ourselves at the fixed-bond approximation and leave the treatment of nuclear motion for work in future.

Figure 6 shows elastic cross sections for the $a^1\Delta_g$ state as functions of electron collision energy. These cross sections have almost the same shape and magnitude as the $X^3\Sigma_g^-$ state elastic cross sections. We do not observe a sharp resonance peak in the $a^1\Delta_g$ elastic cross sections in contrast to the $X^3\Sigma_g^-$ case, because the O_2^- $^2\Pi_g$ resonance is located 0.7 eV below the O_2 $a^1\Delta_g$ state, but 0.2 eV above the $O_2 X^3\Sigma_g^-$ state. As shown in Fig. 6, the $^2\Delta_g$ symmetry is the main contributor to the cross sections at low energy. This indicates that the $l=0$ component of the scattering electron is as important as for the $X^3\Sigma_g^-$ elastic scattering.

The cross section for excitation to the $b^1\Sigma_g^+$ state from the $a^1\Delta_g$ state is shown in Fig. 7. The magnitude of the cross section is about ten times larger than the corresponding cross section for excitation from the $X^3\Sigma_g^-$ state to the $b^1\Sigma_g^+$ state. At electron collision energy of 7.0 eV, there is a large peak in the cross sections arising from the $^2\Pi_u$ symmetry. The origin of this peak is the O_2^- $^2\Pi_u$ resonance as in the cross sections from the $X^3\Sigma_g^-$ state shown in Figs. 3–5. Because the cross sections are plotted as functions of electron colli-
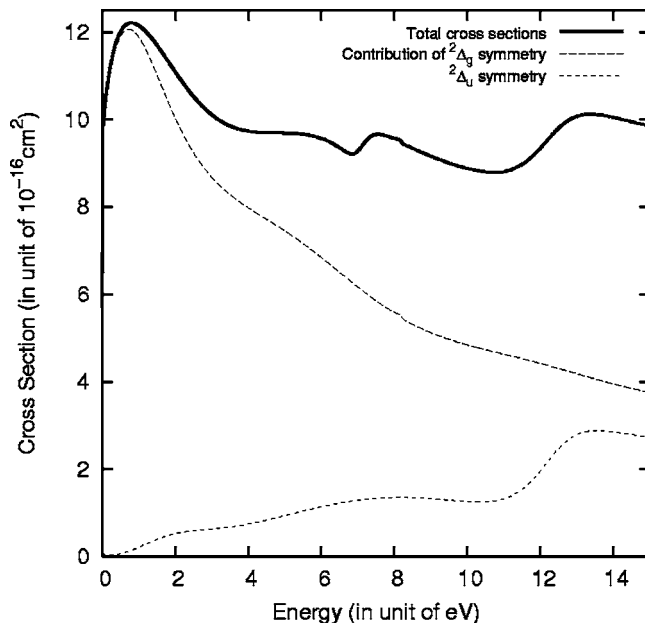
FIG. 6. The elastic cross sections for the $O_2\ a\ ^1\Delta_g$ state. The thick full line represents the cross sections obtained by 13 target states calculation including $1\ ^{1,3}\Pi_{g,u}$ target states. The contributions of the $^2\Delta_g$ and $^2\Delta_u$ total symmetries are also shown.

FIG. 8. Excitation cross sections from the $O_2\ a\ ^1\Delta_g$ state to the 6 eV states of the $O_2\ c\ ^1\Sigma_u^-$, $A'\ ^3\Delta_u$, and $A\ ^3\Sigma_u^+$ states. The cross sections for excitation to the individual state are shown in the thin lines. The thick full line represents the sum of these cross sections.

sion energy, the positions of the peak in Fig. 7 and Figs. 3–5 are different by 0.93 eV which is the energy difference of the $O_2\ X\ ^3\Sigma_g^-$ state and the $O_2\ a\ ^1\Delta_g$ state. Hall and Trajmar experimentally determined differential and integral cross sections at 4.5 eV for this excitation [8]. As in Fig. 7, their value and our results agree well. However, we need more experimental data to make detailed comparisons.
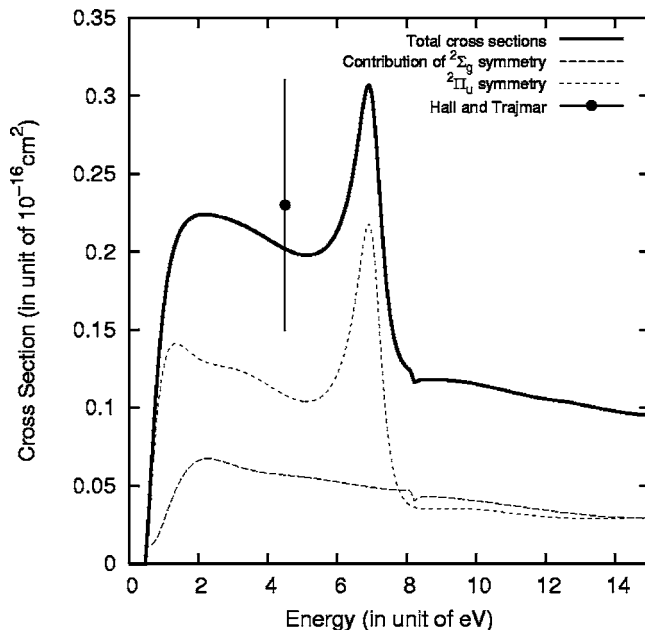
Excitation cross sections to the 6 eV states from the O_2 $a\ ^1\Delta_g$ state are plotted in Fig. 8. There we show the summed cross sections as well as individual contributions of the O_2 $c\ ^1\Sigma_u^-$, $A'\ ^3\Delta_u$, and $A\ ^3\Sigma_u^+$ states. The summed total cross section has a similar shape to the excitation cross section from the $X\ ^3\Sigma_g^-$ state. The origin of a peak at 7.0 eV is the $O_2^-\ ^2\Pi_u$ resonance, as in the case of the $a\ ^1\Delta_g \rightarrow b\ ^1\Sigma_g^+$ transition. The magnitude of the cross sections at this resonance peak is about three times larger than the corresponding cross sections of the $X\ ^3\Sigma_g^-$ case in Fig. 5. The difference is less pronounced in the energy region above 10 eV where the cross sections from the $a\ ^1\Delta_g$ state are about 30% larger than those from the $X\ ^3\Sigma_g^-$ state.

Figures 9 and 10 show the cross sections for electron collisions with the $O_2\ b\ ^1\Sigma_g^+$ excited state. The overall features are quite similar to the corresponding cross sections from the $a\ ^1\Delta_g$ state. In particular, the elastic cross sections of the $b\ ^1\Sigma_g^+$ state in Fig. 9 are almost the same as those of the $a\ ^1\Delta_g$ state shown in Fig. 6. Excitation cross sections to the 6 eV states in Fig. 10 are slightly different from the excitation cross sections to the 6 eV states from the $a\ ^1\Delta_g$ state. The height of the cross section peak at 6.5 eV is about 35% larger than that of the $a\ ^1\Delta_g$case. As in the cases of the $X\ ^3\Sigma_g^- \rightarrow 6$ eV states and $a\ ^1\Delta_g \rightarrow 6$ eV states excitations, the $O_2^-\ ^2\Pi_u$ resonance causes this peak in the cross section. The location of the peak in Fig. 10 is shifted from the peak positions in Figs. 5 and 8 because of energy differences between the $O_2\ X\ ^3\Sigma_g^-$, $a\ ^1\Delta_g$, and $b\ ^1\Sigma_g^+$ states.

Finally, we discuss the effect of the extra $1\ ^3\Pi_{g,u}$ target states in our R-matrix calculations. In Figs. 2–5, we compare cross sections of electron collisions with the $O_2\ X\ ^3\Sigma_g^-$ state from the nine target states calculations and those from the 13 target states calculations including four extra $1\ ^{1,3}\Pi_{g,u}$ target

FIG. 7. Excitation cross section from the $O_2\ a\ ^1\Delta_g$ state to the $b\ ^1\Sigma_g^+$ state. Our results are shown in the thick full line with the contributions of $^2\Sigma_g^+$ and $^2\Pi_u$ symmetries in thin lines as in Fig. 6. The experimental cross section of Hall and Trajmar (see Ref. [8]) is also included for comparison.
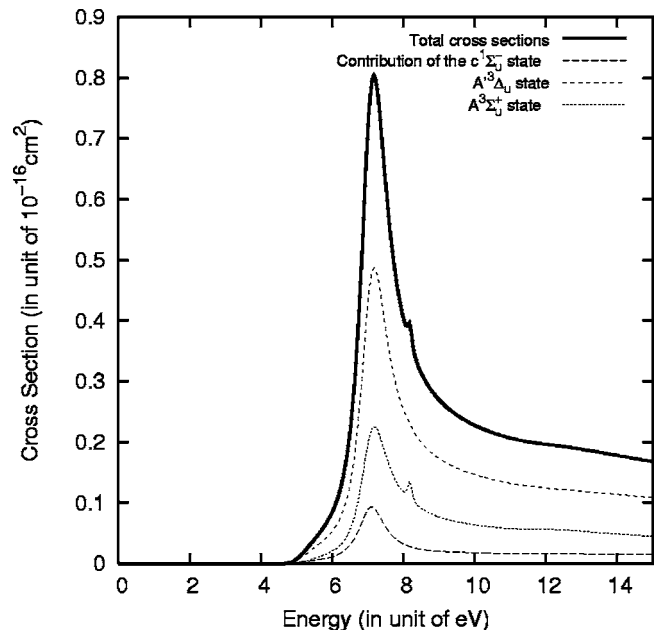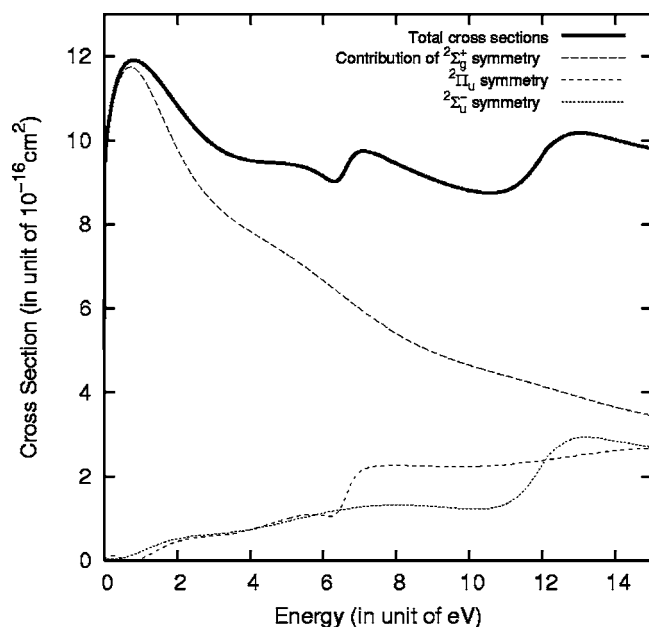
FIG. 9. Elastic cross section for the O_2 $b\,^1\Sigma_g^+$ state. The results are shown in the thick full line with the contributions of $^2\Sigma_g^+$, $^2\Pi_u$, and $^2\Sigma_u^-$ symmetries in the thin lines as in Fig. 6.

FIG. 10. Excitation cross sections from the O_2 $b\,^1\Sigma_g^+$ state to the 6 eV states of the O_2 $c\,^1\Sigma_u^-$, $A'\,^3\Delta_u$, and $A\,^3\Sigma_u^+$ states. The cross sections for excitation to the individual state are shown in the thin lines. The thick full line represents the sum of these cross sections.

states. Inclusion of extra $1\,^{1,3}\Pi_{g,u}$ target states generally lowers the cross sections. However, this lowering is less than 15% and is not significant. Our nine target states cross sections have similar magnitude in general compared to the nine target-states R-matrix calculations of Noble and Burke [18]. However, they are slightly different for the excitations to the $a\,^1\Delta_g$, $b\,^1\Sigma_g^+$ states and 6 eV states in the energy region around 8.0 eV. In this O_2^- $^2\Pi_u$ resonance region, our cross sections are about 20%–30% smaller than their results. These differences in the cross sections may be attributed to the different treatment of the basis set and the CI representations of the target states in ours and their calculations.

IV. SUMMARY

We have investigated electron collisions with the excited $a\,^1\Delta_g$, $b\,^1\Sigma_g^+$ states of the O_2 molecule using the fixed-bond R-matrix method which includes 13 target electronic states, $X\,^3\Sigma_g^-$, $a\,^1\Delta_g$, $b\,^1\Sigma_g^+$, $c\,^1\Sigma_u^-$, $A'\,^3\Delta_u$, $A\,^3\Sigma_u^+$, $B\,^3\Sigma_u^-$, $1\,^1\Delta_u$, $f'\,^1\Sigma_u^+$, $1\,^1\Pi_g$ $1\,^3\Pi_g$ $1\,^1\Pi_u$, and $1\,^3\Pi_u$. These target states are described by CI wave functions in the valence CAS space, using SA-CASSCF orbitals. Gaussian type orbitals are used in this work, in contrast to the STOs in the previous works. Our vertical excitation energies are in good agreement the previous results and the experimental values. We obtain integral cross sections for $a\,^1\Delta_g \rightarrow a\,^1\Delta_g$, $b\,^1\Sigma_g^+$ and 6 eV states
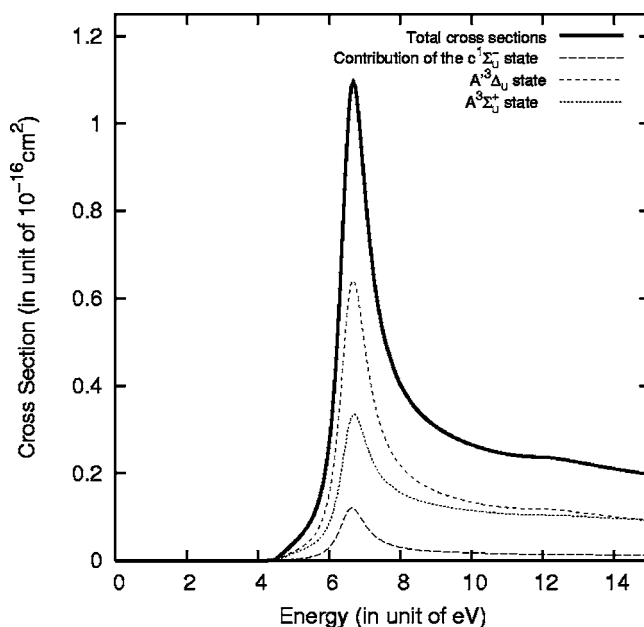
($c\,^1\Sigma_u^-$, $A'\,^3\Delta_u$, and $A\,^3\Sigma_u^+$), as well as $b\,^1\Sigma_g^+ \rightarrow b\,^1\Sigma_g^+$ and 6 eV states. The magnitude of the cross sections for the $a\,^1\Delta_g \rightarrow b\,^1\Sigma_g^+$ transition is consistent with the existing experimental value, which is ten times larger than the one for $X\,^3\Sigma_g^- \rightarrow b\,^1\Sigma_g^+$. The elastic cross sections for the $a\,^1\Delta_g$ state and the $b\,^1\Sigma_g^+$ state have similar magnitude and shape when compared to the elastic cross sections of the $X\,^3\Sigma_g^-$ state. The transitions for the $a\,^1\Delta_g$, $b\,^1\Sigma_g^+ \rightarrow 6$ eV states have cross sections about five times larger than the corresponding transitions from the $X\,^3\Sigma_g^-$ ground state. Our results will be important for modeling of plasma discharge chemistry which needs cross sections between the excited electronic states in some case.

[1] W. E. McDermott, N. R. Pchelkin, D. J. Benard, and R. R. Bousek, Appl. Phys. Lett. **32**, 469 (1978).

[2] D. L. Carroll, J. T. Verdeyen, D. M. King, J. W. Zimmerman, J. K. Laystrom, B. S. Woodard, G. F. Benavides, *et al.*, Appl. Phys. Lett. **86**, 11104 (2005).

[3] D. L. Carroll, J. T. Verdeyen, D. M. King, J. W. Zimmerman, J. K. Laystrom, B. S. Woodard, G. R. Benavides, N. R. Richardson, K. W. Kittell, and W. C. Solomon, IEEE J. Quantum Electron. **41**, 1309 (2005).

[4] M. Shibata, N. Nakano, and T. Makabe, J. Appl. Phys. **80**, 6142 (1996).

[5] J. T. Gudmundsson, J. Phys. D **37**, 2073 (2004).

[6] D. Hayashi and K. Kadota, Jpn. J. Appl. Phys., Part 1 **38**, 225 (1999).

[7] M. J. Brunger and S. J. Buckman, Phys. Rep. **357**, 215 (2002).

[8] R. I. Hall and S. Trajmar, J. Phys. B **8**, L293 (1975).

[9] M. A. Khakoo, W. R. Newell, and A. C. H. Smith, J. Phys. B **16**, L317 (1983).

[10] P. D. Burrow, J. Chem. Phys. **59**, 4922 (1973).

[11] D. S. Belić and R. I. Hall, J. Phys. B **14**, 365 (1981).

[12] D. Teillet-Billy, L. Malegat, and J. P. Gauyacq, J. Phys. B **20**, 3201 (1987).

[13] A. G. Middleton, P. J. O. Teubner, and M. J. Brunger, Phys. Rev. Lett. **69**, 2495 (1992).

[14] A. G. Middleton, M. J. Brunger, M. W. B. A. P. J. O. Teubner, C. J. Noble, G. Wöste, K. Blum, P. G. Burke, and C. Fullerton, J. Phys. B **27**, 4057 (1994).

[15] G. Wöste, C. J. Noble, K. Higgins, P. G. Burke, M. J. Brunger, P. J. O. Teubner, and A. G. Middleton, J. Phys. B **28**, 4141 (1995).

[16] G. Wöste, K. Higgins, P. Duddy, C. M. Fullerton, and D. G. Thompson, J. Phys. B **29**, 2553 (1996).

[17] C. J. Noble and P. G. Burke, J. Phys. B **19**, L35 (1986).

[18] C. J. Noble and P. G. Burke, Phys. Rev. Lett. **68**, 2011 (1992).

[19] K. Higgins, C. J. Noble, and P. G. Burke, J. Phys. B **27**, 3203 (1994).

[20] K. Higgins, C. J. Gillan, P. G. Burke, and C. J. Noble, J. Phys. B **28**, 3391 (1995).

[21] C. J. Noble, K. Higgins, G. Wöste, P. Duddy, P. G. Burke, P. J. O. Teubner, A. G. Middleton, and M. J. Brunger, Phys. Rev. Lett. **76**, 3534 (1996).

[22] J. Tennyson and L. A. Morgan, Philos. Trans. R. Soc. London, Ser. A **357**, 1161 (1999).

[23] P. G. Burke and J. Tennyson, Mol. Phys. **103**, 2537 (2005).

[24] J. D. Gorfinkiel, A. Faure, S. Taioli, C. Piccarreta, G. Halmova, and J. Tennyson, Eur. Phys. J. D **35**, 231 (2005).

[25] R. J. Buenker and S. D. Peyerimhoff, Chem. Phys. Lett. **34**, 225 (1975).

[26] R. J. Buenker and S. D. Peyerimhoff, Chem. Phys. Lett. **8**, 324 (1975).

[27] L. A. Morgan, J. Tennyson, and C. J. Gillan, Comput. Phys. Commun. **114**, 120 (1998).

[28] H.-J. Werner *et al.*, MOLPRO version 2002.6, a package of *ab initio* programs.

[29] T. H. Dunning, J. Chem. Phys. **55**, 716 (1971).

[30] B. K. Sarpal, K. Pfingst, B. M. Nestmann, and S. D. Peyerimhoff, J. Phys. B **29**, 857 (1996).

[31] R. P. Saxon and B. Liu, J. Chem. Phys. **67**, 5432 (1977).

[32] B. F. Minaev and V. A. Minaeva, Phys. Chem. Chem. Phys. **3**, 720 (2001).

[33] A. Faure, J. D. Gorfinkiel, L. A. Morgan, and J. Tennyson, Comput. Phys. Commun. **144**, 224 (2002).

[34] J. Tennyson, J. Phys. B **29**, 1817 (1995).

[35] C. J. Gillan, C. J. Noble, and P. G. Burke, J. Phys. B **21**, L53 (1988).

[36] J. D. Gorfinliel and J. Tennyson, J. Phys. B **38**, 1607 (2005).

[37] J. P. Gauyacq, D. Teillet-Billy, and L. Malegat, in *Electron-Molecule Scattering and Photodissociation*, edited by P. G. Burke and J. B. West (Plenum, New York, 1988), pp. 213–219.

[38] M. A. Green, P. J. O. Teubner, M. J. Brunger, D. C. Cartwright, and L. Campbell, J. Phys. B **34**, L157 (2001).

[39] S. Trajmar, D. C. Cartwright, and W. Williams, Phys. Rev. A **4**, 1482 (1971).

[40] I. Kanik, S. Trajmar, and J. C. Nickel, J. Geophys. Res. **98**, 7447 (1993).

[41] T. W. Shyn and W. E. Sharp, Phys. Rev. A **26**, 1369 (1982).

[42] J. P. Sullivan, J. Gibson, R. J. Gulley, and S. J. Buckman, J. Phys. B **28**, 4319 (1995).

[43] I. Linert, G. C. King, and M. Zubek, J. Phys. B **37**, 4681 (2004).

[44] J. P. Doering, J. Geophys. Res. **97**, 12267 (1992).

[45] T. W. Shyn and C. J. Sweeney, Phys. Rev. A **47**, 1006 (1993).

[46] D. Teillet-Billy, L. Malegat, J. P. Gauyacq, R. Abouaf, and C. Benoit, J. Phys. B **22**, 1095 (1989).